Multi-Antenna Noncoherent ML Synchronization for UWB-IR Faded Channels

Enzo Baccarelli, Mauro Biagi, Cristian Pelizzoni, and Nicola Cordeschi

Abstract: **This contribution focuses on the maximum likelihood (ML) noncoherent synchronization of multi-antenna transceivers working in faded environments and employing ultra-wideband impulse radio (UWB-IR) transmit technology. In particular, the Cramer-Rao bound (CRB) is derived for the general case of multiple input multiple output (MIMO) UWB-IR systems and used to compare the ultimate performance of three basic transmit schemes, thereinafter referred to as single input multiple output (SIMO), MIMO equal signaling (MIMO-ES), and MIMO orthogonal signaling (MIMO-OS) ones. Thus, the noncoherent ML synchronizer is developed for the better performing transmit scheme (i.e., the SIMO one) and its performance is evaluated under both signal acquisition and tracking operating conditions. The performance gain in the synchronization of UWB-IR signals arising by the utilization of the multi-antenna technology is also evaluated.**

Index Terms: **Cramer-Rao bound (CRB), multi-antenna, multiple input multiple output (MIMO) fading channels, noncoherent maximum likelihood (ML) synchronization, ultra-wideband impulse radio (UWB-IR).**

I. INTRODUCTION

Ultra-wideband impulse radio (UWB-IR) for commercial communications is a quite recent proposal [1]. UWB-IR transmitters work at baseband and employ short carrierless pulses at (very) low power with (very) large bandwidths of up to or more than several GHz [1]. The UWB-IR technology presents several attractive features stemming from its UWB nature. Specifically, it can achieve processing gains larger than those of typical direct sequence spread spectrum (DS-SS) systems [2] and can also offer extremely fine time resolution. Thus, a distinguishing feature of UWB-IR systems is the use of baseband data modulation techniques suited for power-limited applications with (extremely) large bandwidths as, for example, orthogonal pulse position modulation (OPPM). The application scenarios we consider are emerging high throughput outdoor 4G-WLANs [3], [4]. The choice of UWB-IR transmission scheme is justified by the recent agreement in IEEE 802.15.3a working group about the technique to be adopted for UWB transmissions [5]. At the present, several non minor challenges are still to be won to deploy high performance 4G-WLANs based on the UWB-IR technology [6]. Among other challenges, we mention that due to both the baseband nature of the transmitted pulse position modulation (PPM) signals and the (very) high frequencies covered by the corresponding spectra, the coverage range of current UWB-IR systems is limited up to few meters [3], [7]. Furthermore, the short duration (below the nanosecond) of the transmitted UWB pulse requires very reliable timing acquisition and tracking (e.g., robust synchronization recovery) at the receiver, specially when multi-level PPM formats are employed [8]–[11].

A. *Previous Works on the Synchronization of UWB Systems and Actual Contribution*

An overview of the many contributions published about the synchronization of UWB systems shows that all these works focus on single antenna (e.g., single input single output (SISO)) transceivers and none of them tackles multi-antenna systems. Specifically, among other contributions, the topic of the signal acquisition for SISO UWB systems has been recently afforded, for example, in [12]–[16]. Training pulses are transmitted in [12] for channel estimation which, in turns, are exploited for timing acquisition. In order to reduce the receiver complexity, the procedure developed in [13] starts with a coarse acquisition and then iteratively reduces the searching window so to refine the final fine timing acquisition. Synchronizers based on the maximum likelihood (ML) principle have been developed in [14], [15] for SISO UWB systems impaired by multi-path phenomena, while a time acquisition scheme based on the minimization of the false alarm probability has been proposed in [16] for SISO UWB transceivers affected by multiple access interference. Passing now to consider the topic of the signal tracking, this last has been recently investigated for SISO UWB transceivers in [8], [9], [17], [18]. Specifically, in [17] the effects of the shape of the UWB pulse on the timing jitter have been pointed out, while in [18] the capacity loss of the network (measured in terms of the maximum number of allowed users) is evaluated as a function of the overall time jitter introduced by both receive and transmit clocks. An analytical tool for evaluating the sensitivity of SISO UWB transceivers on the clock jitter has been developed in [8], while the performance loss induced by jitter in multi-path faded applications is evaluated in [9]. Dealing with multi-antenna synchronization, performances are evaluated in the presence of antenna array and by considering carrier-modulated signals in [19]. This contribution focuses on the optimized design and performance evaluation of synchronization modules (based on the ML estimation principle) for single user[1] multiple input multiple output (MIMO) UWB-IR systems affected by flat fading and thermal noise. Since timing acquisition is the first task to be accomplished by the multi-antenna receiver when it is turned on, we assume that no knowledge about actual values of the fading coefficients of the MIMO

Manuscript received January 14, 2005; approved for publication by Yong-Hoon Lee, Division I Editor, January 24, 2006.

The authors are the with INFOCOM Department, University of Rome "La Sapienza," via Eudossiana 18, 00184 Rome, Italy, email: {enzobac, biagi, pelcris, cordeschi}@infocom.uniroma1.it.

[1]The effects of the multiple access interference (MAI) have been recently addressed in [4], where a MAI resistant adaptive codec for UWB-IR terminals is proposed.

channel is available at the receiver for timing acquisition, so that we qualify as "noncoherent" the resulting ML synchronizer. Specifically, the main contributions of this paper may be so summarized.

- We develop the Cramer-Rao bound (CRB) for the ML estimation of the delay (e.g., timing) parameter for MIMO UWB-IR transceivers when the receiver is fully *unaware* about actual values assumed by the faded coefficients of the underlying MIMO channels (e.g., noncoherent reception is assumed).
- Since the obtained CRB does not give direct insight about the optimal transmit scheme to be used, we evaluate and compare the CRBs corresponding to three basic transmit schemes of practical interest, referred to as single input multiple output (SIMO), MIMO equal signaling (MIMO-ES), and MIMO orthogonal signaling (MIMO-OS) schemes.
- We give evidence that the SIMO scheme is the most performing out of the considered ones, and then we develop for this last both the corresponding ML equation for the (noncoherent) timing recovery and the related ML (noncoherent) synchronizer.
- We show that at medium/high SNRs the proposed ML synchronizer achieves the CRB and converges (in the almost surely sense) to the actual value assumed by the (a priori unknown) timing parameter.
- We present some results about the optimized tuning of the loop filter (LF) to be used by the proposed ML synchronizer.

The paper is organized in the following way. After the description of the considered MIMO UWB-IR system model in Section II, in Section III we present the general formula of the CRB for the noncoherent timing estimation in the presence of slow-variant flat fading phenomena, and we compare the CRBs corresponding to three transmit schemes of practical interest (namely, the SIMO, MIMO-ES, and MIMO-OS ones). In Section IV, we derive the ML equation for the best (in the sense of lowest CRB) transmit scheme (i.e., the SIMO one) and point out some of its asymptotic properties. Then, we develop the corresponding ML noncoherent synchronizer and stress some results about the optimized setting of the LF in Section V. Several numerical plots testing the actual performance of the proposed synchronizer under both signal acquisition and tracking operating conditions are presented in Section VI, while in the final Section VII we introduce and (shortly) address some open problems. About the adopted notation, bold capital letters denote matrices, bold lower-case underlined symbols indicate vectors, while non-bold characters are used for scalar quantities. Furthermore, $(\cdot)^T$ means transposition, lg indicate the natural logarithm, det[**A**] is the determinant of matrix **A**, $\mathbf{I}_L$ is the $(L \times L)$ identity matrix, Tra[**A**] is the trace of **A**, $\underline{\mathbf{1}}_m$ is the $(m \times 1)$ column vector with all entries equal to unit, $\underline{\mathbf{0}}_m$ is the $(m \times 1)$ zero vector, while $\mathbf{0}_L$ is the $(L \times L)$ zero matrix.

II. THE CONSIDERED MIMO UWB-IR SYSTEM MODEL

Let us consider a baseband peer-to-peer UWB-IR MIMO wireless system impaired by slow-variant flat fading phenomena and equipped with $N_t \geq 1$ transmit and $N_r \geq 1$ receive antennas. By assuming non-line-of-sight (NLOS) application scenarios, as in [3], [7], [20], the path gain h_{ji} from transmit antenna i to receive antenna j may be modeled as a zero-mean unit-variance real Gaussian random variable[2] (r.v.) and the $(N_t \times N_r)$ path gains $\{h_{ji} \in \mathbb{R}^1, 1 \leq j \leq N_r, 1 \leq i \leq N_t\}$ may be considered mutually independent.[3] We consider a packet transmission system where each packet is composed by a (known to the receiver) synchronization trailer field, followed by the header and payload fields; as in [6], [16], we assume that the timing acquisition must be performed at the beginning of each transmitted packet by exploiting the trailer field and then time tracking is carried out over the remaining parts (e.g., header plus payload) of the packet. Since high throughput multi-antenna WLANs are typically planned for low mobility applications involving nomadic (e.g., quasi-static) user terminals, the corresponding MIMO channel may be considered time invariant at least over the overall duration of each packet, but is allowed to vary over multiple packets [3], [7], [20]. Thus, since the above mentioned path gains $\{h_{ji}\}$ may be considered constant during the transmission of the trailer field, the (baseband real) signal $r_j(t)$ measured at the output of the j-th receive antenna over the time window $[-T_0, T_0]$ corresponding to the transmission of the trailer field may be modeled as

$$r_j(t) = \sum_{i=1}^{N_t} h_{ji} x_i(t+\tau) + n_j(t), \quad t \in [-T_0, T_0], \quad j = 1, \cdots, N_r \tag{1}$$

where τ is the *unknown* delay to be estimated, while $\{n_j(t) \in \mathbb{R}^1, j = 1, \cdots, N_r\}$ are mutually independent zero-mean Gaussian white noises with unit two-sided power density spectrum (e.g., $\mathcal{N}_0/2 = 1$ (watt/Hz)). About (1), we assume that the (unknown) delay τ falls into the interval $[-\bar{\tau}_{\max}, \bar{\tau}_{\max}]$, where $\bar{\tau}_{\max}$ is the maximum expected delay that may be evaluated in advance as in $\bar{\tau}_{\max} = R/c$, where R(m) is the coverage range of the system and $c = 3 \times 10^8$(m/sec) is the speed of the light. Furthermore, $x_i(t)$ in (1) is the (real-valued baseband) signal radiated by i-th transmit antenna during the trailer phase, and according to

$$x_i(t) = \sqrt{\frac{\mathcal{E}}{N_t}} \sum_{m=-N_S/2}^{N_S/2} s^{(i)}(t - 4m\bar{\tau}_{\max}), \quad t \in [-T_0, T_0], \quad i = 1, \cdots, N_t. \tag{2}$$

We assume that $x_i(t)$ is composed by a train of $(N_S + 1)$ non overlapping pulses $\{s^{(i)}(t - 4m\bar{\tau}_{\max}), m = 0, \pm 1, \cdots, \pm N_S/2\}$ time shifted apart by multiple of $4\bar{\tau}_{\max}$. In particular, we assume that the baseband pulse $s^{(i)}(t)$ employed by i-th trans-

[2] As is well known, the flat fading assumption requires that the (half-power) bandwidth of the transmitted UWB pulse is below the coherence bandwidth of the MIMO channel. Although the bandwidth of the UWB pulse may be over 1 GHz for outdoor microcellular applications, the flat-faded assumption may be considered reasonably met [20], [21]. Some results about the optimized design of multi-path impaired UWB systems have been recently reported in [22]. In addition, this channel model is also considered in [20] and it may be considered suitable [19] for the UWB-IR transmission format (this transmission technique has been chosen by the IEEE 802.15.3a working group) when NLOS outdoor propagation scenario is taken into account.

[3] As pointed out in [23], this assumption is met in WLAN applications for an antenna spacing of the order of $\lambda/2$, where λ is the wavelength of the radiated UWB pulse evaluated at the center frequency of the corresponding spectrum.

mit antenna has *unit-energy* and spans the time interval $t \in [-\bar{\tau}_{\max}, \bar{\tau}_{\max}]$.[4] As consequence, in order to capture at the receiver the overall energy conveyed by the observed signals in (1), the corresponding time window T_0 of the system must (at least) equate

$$T_0 = 2(1 + N_S)\bar{\tau}_{\max}. \tag{3}$$

Finally, being $\mathcal{E}$ (joule) in (2) the total energy radiated by all N_t transmit antennas over the duration $2\bar{\tau}_{\max}$ of each pulse, the resulting SNR per pulse γ measured at the output of each receive antenna equates $\gamma = \mathcal{E}$, regardless of the number N_t of employed transmit antennas. Before proceeding, it is worthwhile to stress that since the duration of $s^{(i)}(t), i = 1, \cdots, N_t$, is limited to $[-\bar{\tau}_{\max}, +\bar{\tau}_{\max}]$, we have the following orthogonality property

$$\int_{-T_0}^{T_0} s^{(i)}(t - 4m\bar{\tau}_{\max}) s^{(i)}(t - 4l\bar{\tau}_{\max} + \Delta) dt = \begin{cases} 1, \text{ for } l = m \text{ and } \Delta = 0, \\ 0, \text{ for } l \neq m \text{ and } |\Delta| \leq 2\bar{\tau}_{\max} \end{cases} \tag{4}$$

so that the $(1 + N_S)$ components of the train in (2) and their Δ-shifted versions are orthogonal over the system time window $[-T_0, T_0]$.

III. THE CRAMER-RAO BOUND (CRB) FOR MIMO SIGNALING AND NON COHERENT SYNCHRONIZATION

Our first task is to compute the CRB on the synchronization error of the considered MIMO UWB-IR system, so to gain insight about the ultimate achievable performance of the synchronizer we develop in the following section. For this purpose, after indicating as $\dot{s}^{(i)}(t)$ and $\ddot{s}^{(i)}(t)$ the first and second time derivatives of the pulse $s^{(i)}(t)$, let us denote as

$$\varepsilon_{ss}(i,j) \triangleq \int_{-T_0}^{T_0} s^{(i)}(t) s^{(j)}(t) dt,$$

$$\varepsilon_{\dot{s}s}(i,j) \triangleq \int_{-T_0}^{T_0} \dot{s}^{(i)}(t) s^{(j)}(t) dt$$

and

$$\varepsilon_{\dot{s}\dot{s}}(i,j) \triangleq \int_{-T_0}^{T_0} \dot{s}^{(i)}(t) \dot{s}^{(j)}(t) dt, \qquad 1 \leq i, j \leq N_t$$

the resulting cross-energies.[5] Afterwards, let us indicate as $\mathbf{Q}_0$ the symmetric semidefinite-positive $(N_t \times N_t)$ matrix whose (i,j)-th entry is $\varepsilon_{ss}(i,j)$, while $\mathbf{Q}_1$ denotes the corresponding $(N_t \times N_t)$ matrix with (i,i)-th entry equal to $\varepsilon_{\dot{s}s}(i,j)$. Finally, let $\mathbf{Q}_2$ be the $(N_t \times N_t)$ symmetric definite-positive matrix with the (i,j)-th given by $\varepsilon_{\dot{s}\dot{s}}(i,j)$. Thus, under the assumption that the receiver is fully unaware about actual values assumed by the MIMO channel coefficients $\{h_{ji}\}$, it is proved in the Appendix I that the CRB for the (unbiased) estimate of the delay parameter τ assumes the following (compact) form

$$\sigma_\epsilon^2(\tau) \triangleq E\{(\tau - \hat{\tau})^2\} \geq \left\{ \left(\frac{\gamma(1 + N_S)}{N_t} \right)^2 N_r \times \mathrm{Tra} \left\{ \left[\mathbf{Q}_2 \mathbf{Q}_0^T - \mathbf{Q}_1 \mathbf{Q}_1^T \right] \left[\mathbf{I}_{N_t} + \frac{\gamma(1 + N_S)}{N_t} \mathbf{Q}_0 \right]^{-1} \right\} \right\}^{-1} (\text{sec}^2) \tag{5}$$

where the expectation in (5) is with respect to the joint pdf of the received signals in (1) conditional on the actual value τ assumed by the delay parameter. Therefore, after accounting for the energy constraints $\varepsilon_{ss}(i,i) = 1$ and $\varepsilon_{\dot{s}s}(i,i) = 0$ (see Footnote 5), it can be viewed that the above bound depends on the

$$N_t(2N_t - 1) \tag{6}$$

values assumed by the cross-energies constituting the entries of the $\mathbf{Q}_0, \mathbf{Q}_1$, and $\mathbf{Q}_2$ matrices. Hence, from a system design perspective, the key problem is to set these cross-energies so as to *minimize* the value assumed by the CRB in (5); this is equivalent to designing the optimized MIMO signaling format for the estimation of the delay parameter. Unfortunately, this problem seems to resist closed form analytical solution, even in the simplest case of $N_t = 2$ transmit antennas. So, to bypass this Gordian Knot, we attempt to approach the problem under a somewhat different perspective. Specifically, in the following subsections we evaluate (and compare) the values assumed by the CRB in (5) in correspondence of three schemes of practical interest and then in Section IV we proceed to develop the ML synchronizer.

A. The CRB for the SIMO System

Let us start to consider a single antenna (e.g., $N_t = 1$) transmitter, so that only the first transmit antenna is turned on and radiates the following signal (see (1) for $N_t = 1$)

$$x^{(1)}(t) = \sqrt{\gamma} \sum_{m=-N_S/2}^{m=N_S/2} s(t - 4m\bar{\tau}_{\max}), \quad t \in [-T_0, T_0]. \tag{7}$$

Since in this case the matrices $\mathbf{Q}_0, \mathbf{Q}_1$, and $\mathbf{Q}_2$ reduce to scalar entities assuming the values 1, 0, and $\varepsilon_{\dot{s}} \triangleq \varepsilon_{\dot{s}\dot{s}}(1,1)$, respectively, the resulting CRB in (5) becomes

$$\sigma_\epsilon^2(\tau) \geq \frac{1 + \gamma(1 + N_S)}{\varepsilon_{\dot{s}} N_r (\gamma(1 + N_S))^2} (\text{sec}^2). \tag{8}$$

About the above bound the following remarks are in order.

Remark 1 (On the optimized pulse)

The (unit-energy) optimized pulse $s(t)$ minimizing (8) must maximize the energy $\varepsilon_{\dot{s}}$ of the corresponding time derivative signal. As is well known [24]–[26], under the constraint on the peak value allowed $s(t)$, the maximal $\varepsilon_{\dot{s}}$ is achieved by a triangular-shaped pulse. □

Remark 2 (Coherent vs. noncoherent synchronization)

[4] We anticipate that the above assumption about the duration of $s^{(i)}(t), i = 1, \cdots, N_t$, together with the time shifts of multiple of $4\bar{\tau}_{\max}$ in (2) guarantees that the ML estimate $\hat{\tau}_{ML}$ in (13) of the delay τ is exact, at least for vanishing $\mathcal{N}_0$ (e.g., $\hat{\tau}_{ML} = \tau$ for $\mathcal{N}_0 \to 0$; see the Proposition 1 in Section III). This property is *no longer retained* when pulses $s^{(i)}(t)$ narrower than $2\bar{\tau}_{\max}$ and/or time shifts shorter than $4\bar{\tau}_{\max}$ are employed in (2).

[5] Obviously, $\varepsilon_{\dot{s}s}(i,i) = 0$ for any i, while $\varepsilon_{ss}(i,i) = 1$ for any i due to the above assumption of unit-energy pulses.

When all the SIMO channel coefficients $\{h_{j1}, j = 1 \cdots, N_r\}$ in (1) are assumed known (that is, perfectly estimated) at the receiver, it can be proved that the resulting CRB becomes

$$\sigma_\epsilon^2(\tau) \geq \{N_r \varepsilon_{\dot{s}} \gamma(1 + N_S)\}^{-1} \ (\text{sec}^2). \tag{8.1}$$

Thus, by comparing (8) with (8.1), we conclude that the SNR loss induced in the CRB by lack of knowledge of the SIMO channel coefficients equates $[1 + \gamma(1 + N_S)]/\gamma(1 + N_S)$. This loss grows unbounded for $\gamma \to 0$, while approaches unit for $\gamma \to \infty$. □

E. The CRB for MIMO Systems with Equal Signaling (MIMO-ES)

As a second transmit scheme, let us assume that all the $N_t \geq 2$ transmit antennas employ a same pulse $s(t)$, so to have in (5)

$$s^{(i)}(t) \equiv s(t), \quad i = 1, \cdots, N_t. \tag{9}$$

In this case, the $(N_t \times N_t)$ matrices involved by the bound in (5) become

$$\mathbf{Q}_0 = \underline{\mathbf{1}}_{N_t}(\underline{\mathbf{1}}_{N_t})^T; \ \mathbf{Q}_1 = \mathbf{0}_{N_t}; \ \mathbf{Q}_2 = \varepsilon_{\dot{s}} \underline{\mathbf{1}}_{N_t}(\underline{\mathbf{1}}_{N_t})^T.$$

Thus, since the resulting CRB assumes the same expression previously reported in (8) for the SIMO system[6]

$$\sigma_\epsilon^2(\tau) \geq [1 + (1 + N_S)\gamma]/[N_r \varepsilon_{\dot{s}}(\gamma(1 + N_S))^2] \tag{10}$$

we conclude that from a synchronization performance point view, the MIMO-ES transmit scheme in (9) does not offer any improvement over the above SIMO scheme of (7).

C. The CRB for MIMO Systems with Orthogonal Signaling (MIMO-OS)

As third signaling scheme, let us assume that the $N_t \geq 2$ pulses $s^{(i)}(t), i = 1, \cdots, N_t$ employed by the transmit antennas are mutually orthogonal over the interval $[-T_0, T_0]$ for any time shift $\Delta \in [-2\bar{\tau}_{\max}, 2\bar{\tau}_{\max}]$, so to satisfy the following relationship

$$\int_{-T_0}^{T_0} s^{(i)}(t) s^{(j)}(t + \Delta) dt = 0, \quad \forall \ | \Delta | \leq 2\bar{\tau}_{\max}, \forall \, i \neq j. \tag{11}$$

Under this assumption, also the overall signals $x^{(i)}(t)$ in (2), $i = 1, \cdots, N_t$, radiated by the transmit antennas are orthogonal over $[-T_0, T_0]$ for any time shift $| \Delta | \leq 2\bar{\tau}_{\max}$. Thus, since the resulting $\mathbf{Q}_0$ and $\mathbf{Q}_1$ matrices equate $\mathbf{I}_{N_t}$ and $\mathbf{0}_{N_t}$, respectively, the corresponding CRB in (5) now becomes

$$\sigma_\epsilon^2(\tau) \geq [N_t + \gamma(1 + N_S)]/[N_r \bar{\varepsilon}_{\dot{s}}(\gamma/(1 + N_S))^2] \quad (\text{sec}^2) \tag{12}$$

where

$$\bar{\varepsilon}_{\dot{s}} \triangleq \frac{1}{N_t} \text{Tra}\{\mathbf{Q}_2\} \equiv \frac{1}{N_t} \sum_{i=1}^{N_t} \varepsilon_{\dot{s}\dot{s}}(i, i)$$

[6](10) follows from an application of the Sherman-Morrison formula to compute the inverse matrix $[\mathbf{I}_{N_t} + (1 + N_S)\frac{\gamma}{N_t} \ \underline{\mathbf{1}}_{N_t}(\underline{\mathbf{1}}_{N_t})^T]^{-1}$.

is the average energy of the time derivative pulses $\dot{s}^{(i)}(t), i = 1, \cdots, N_t$. Thus, a comparison of (8) with (12) shows that at $\varepsilon_{\dot{s}} = \bar{\varepsilon}_{\dot{s}}$, the SNR loss paid by the MIMO-OS scheme in (11) over the SIMO one in (7) equates $[N_t + \gamma(1 + N_S)]/[1 + \gamma(1 + N_S)]$. Therefore, this loss approaches N_t for $\gamma \to 0$, while it reduces to unit for $\gamma \to \infty$. As a consequence, from a synchronization performance point of view, there *is no reason to prefer* the MIMO-OS scheme over the SIMO one. Overall, from the carried out performance comparison, we conclude that the SIMO scheme in (7) outperforms the MIMO-ES and MIMO-OS ones in (9) and (11), so that in the following section we focus on the development of the ML (noncoherent) synchronizer for the SIMO scheme.

IV. ML DELAY ESTIMATION FOR SIMO SYSTEMS

The ML estimate $\hat{\tau}_{ML}$ of the delay parameter τ affecting the SIMO system in (7) is given by the following (definitory) relationship

$$\hat{\tau}_{ML} \triangleq \underset{\tau \epsilon [-\bar{\tau}_{\max}, \bar{\tau}_{\max}]}{\arg\max} \{\lg p(\underline{r}_1, \cdots, \underline{r}_{N_t} \mid \tau)\} \overset{(a)}{=} \underset{\tau \epsilon [-\bar{\tau}_{\max}, \bar{\tau}_{\max}]}{\arg\max}$$

$$\times \left\{ \sum_{j=1}^{N_r} \left(\sum_{m=-N_S/2}^{N_S/2} \int_{-T_0}^{T_0} r_j(t) s(t - 4m\bar{\tau}_{\max} + \tau) dt \right)^2 \right\} \tag{13}$$

where (a) directly follows from the expression in (A.6) for the conditional joint pdf $p(\underline{r}_1, \cdots, \underline{r}_{N_t} \mid \tau)$ of the received signals in (1). Since at low/medium SNR γ the pdf in (A.6) does not assume the exponential form reported by (IV.C.32) of [26], we conclude that at low/medium SNRs the performance of the ML estimate in (13) does not achieve the CRB in (8) (see [26, p. 177] for more details on this general question).

Proposition 1 (Asymptotic performance of the ML estimator) Let us assume that the pulse $s(t)$ in (7) spans the time interval $[-\bar{\tau}_{\max}, \bar{\tau}_{\max}]$. Thus, for large $\gamma(1 + N_S)$, the ML estimate in (13) converges (in the almost surely sense) to the actual value τ of the delay parameter, according to the following limit

$$\lim_{\gamma(1+N_S) \to \infty} \hat{\tau}_{ML} = \tau.$$

□

Therefore, the above property guarantees that, for large $\gamma(1 + N_S)$ values, the ML estimate in (13) achieves the CRB in (13). In this regard, we have analytically ascertained that the mean squared error $E\{(\tau - \hat{\tau}_{\max})^2\}$ of the ML estimate *closely* approaches the CRB in (13) for

$$\gamma > 4/[a(2 + N_r)(1 + N_S)] \tag{14}$$

where the constant a is defined as

$$a \triangleq \frac{1}{2\bar{\tau}_{\max}} \int_0^{2\bar{\tau}_{\max}} \rho_{ss}^2(\Delta) d\Delta$$

with $\rho_{ss}^2(\Delta)$ being the autocorrelation function of the pulse $s(t)$ present in (7). The performance plots of Section VI confirm, indeed, this conclusion.

A. The ML Equation

By equating to zero (A.7), we obtain the so-called ML equation that for the SIMO system in (7) assumes the following form

$$\sum_{j=1}^{N_r}\sum_{k=-N_S/2}^{N_S/2}\sum_{l=-N_S/2}^{N_S/2}\left(\int_{-T_0}^{T_0} r_j(t)s(t-4k\bar{\tau}_{\max}+\hat{\tau})dt\right) \times\left(\int_{-T_0}^{T_0} r_j(t)\dot{s}(t-4l\bar{\tau}_{\max}+\hat{\tau})dt\right)=0. \quad (15)$$

Obviously, before using (16) for computing the ML estimate $\hat{\tau}_{ML}$ defined in (13), we must ascertain that $\hat{\tau}_{ML}$ is the *unique* solution of (16).

Proposition 2 (Asymptotic behavior of the ML equation) Let us indicate as

$$\rho_{ss}(\Delta)\triangleq\int_{-T_0}^{T_0} s(t)s(t+\Delta)dt,$$
$$\chi_{s\dot{s}}(\Delta)\triangleq\int_{-T_0}^{T_0} s(t)\dot{s}(t+\Delta)dt \quad (16)$$

the autocorrelation function of the employed pulse $s(t)$ and the corresponding cross-correlation function among $s(t)$ and its time derivative $\dot{s}(t)$. Let us assume that the following two conditions are met.

i) $\rho_{ss}(\Delta)$ does not vanish for $|\Delta|\leq 2\bar{\tau}_{\max}$;

ii) $\chi_{s\dot{s}}(\Delta)$ vanishes only at $\Delta=0$ over the interval $\Delta\in[-2\bar{\tau}_{\max},2\bar{\tau}_{\max}]$.

Thus, for large $\gamma(1+N_S)$, the solution $\hat{\tau}$ of the ML equation in (16) is *unique* and converges (in the almost surely sense) to the actual value τ of the delay parameter, so that we can write

$$\lim_{\gamma(1+N_S)\to\infty}\hat{\tau}=\tau. \quad (17)$$

□

Remark 3 (On the asymptotic performance of the ML estimator)
The Conditions *i)* and *ii)* of the Proposition 2 *suffice* to guarantee that at high SNRs the solution $\hat{\tau}$ of the ML equation (16) coincides (almost surely) with the ML estimate $\hat{\tau}_{ML}$ that, in turn, converges to the true value τ at high SNRs (see the Proposition 1). As a consequence, we conclude that when the above Conditions *i)* and *ii)* are met, the resulting mean square error $E\{\tau-\hat{\tau}^2\}$ affecting the solution $\hat{\tau}$ of (16) *vanishes at high SNRs*, and this is confirmed, indeed, by the numerical plots of Section VI, where *no* MSE floors are present. Specifically, we have analytically ascertained that, under the above Conditions *i)* and *ii)*, the solution $\hat{\tau}$ of (16) closely approaches the corresponding true value τ at an SNR γ satisfying the following inequality.

$$\gamma>(1+\varepsilon_{\dot{s}})/[(1+N_S)(2+N_r)b] \quad (18)$$

with the b constant defined as in

$$b\triangleq(1/\bar{\tau}_{\max})\int_0^{\bar{\tau}_{\max}}(\chi_{s\dot{s}}(\Delta))^2\,d\Delta.$$

However, as also pointed out in [27, Sections 7.4.2 and 7.4.3], we experienced that, when the above Conditions *i)* and *ii)* fall short, the asymptotic convergence of the solution $\hat{\tau}$ of (16) to the true value τ is no longer guaranteed, so that the resulting performance plots of the ML estimator (16) may present MSE floors. □

Remark 4 (On the shape of the employed pulse)
The commonly adopted (unit-energy) pulse $s(t)$ in current UWB-IR data transmission systems is modeled as the second derivative of the Gaussian function and is formally defined as [2]

$$s(t)\equiv\sqrt{\frac{8}{3T_s}}\left[1-4\pi\left(\frac{t}{T_s}\right)^2\right]\exp\left(-2\pi\left(\frac{t}{T_s}\right)^2\right) \quad (19)$$

where T_s(sec) is the so-called "shaping factor" of the pulse. Now, for $\Delta\neq 0$ the autocorrelation and cross-correlation functions of this pulse

$$\rho_{ss}(\Delta) = \frac{1}{12}\exp\left(-\pi\left(\frac{\Delta}{T_s}\right)^2\right)H_4\left(\sqrt{\pi}\frac{|\Delta|}{T_s}\right),$$
$$\chi_{s\dot{s}}(\Delta) = \frac{1}{12\sqrt{2}}\exp\left(-\pi\left(\frac{\Delta}{T_s}\right)^2\right)H_5\left(\sqrt{\pi}\frac{\Delta}{T_s}\right)$$

vanish in the correspondence of the zeros of the 4th and 5th order Hermite polynomials $H_4(\cdot)$ and $H_5(\cdot)$. Thus, in order to satisfy the conditions of Proposition 2, it should be (carefully) checked that no zero of $H_4(\cdot)$ falls in the interval $[-2\bar{\tau}_{\max},2\bar{\tau}_{\max}]$ and only the zero at $\Delta=0$ of $H_5(\cdot)$ falls in this interval. Otherwise, the above stated convergence property of the solution of the ML equation is no longer guaranteed. □

V. THE NON COHERENT ML SYNCHRONIZER

An appealing feature of the ML equation in (16) is that, in practice, it may be implemented via a suitable "early-late gate" architecture. So, the ML equation in (16) may be equivalently rewritten as (see Appendix II)

$$e(\hat{\tau})=0 \quad (20)$$

where the error signal $e(\hat{\tau})$ depends on the current estimate output by the synchronizer and it is defined as

$$e(\hat{\tau}) \triangleq -\sum_{j=1}^{N_r}\left(\int_0^{2T_0} r_j(t+T_0)v(t+\hat{\tau})dt\right) \times\left(\int_0^{2T_0} r_j(t+T_0)v(t+\hat{\tau}-\mu)dt\right) +\sum_{j=1}^{N_r}\left(\int_0^{2T_0} r_j(t+T_0)v(t+\hat{\tau})dt\right) \times\left(\int_0^{2T_0} r_j(t+T_0)v(t+\hat{\tau}+\mu)dt\right) \quad (21)$$

with

$$v(t)\triangleq\sum_{k=1}^{1+N_S} s(t+4k\bar{\tau}_{\max}-2\bar{\tau}_{\max}) \quad (22)$$

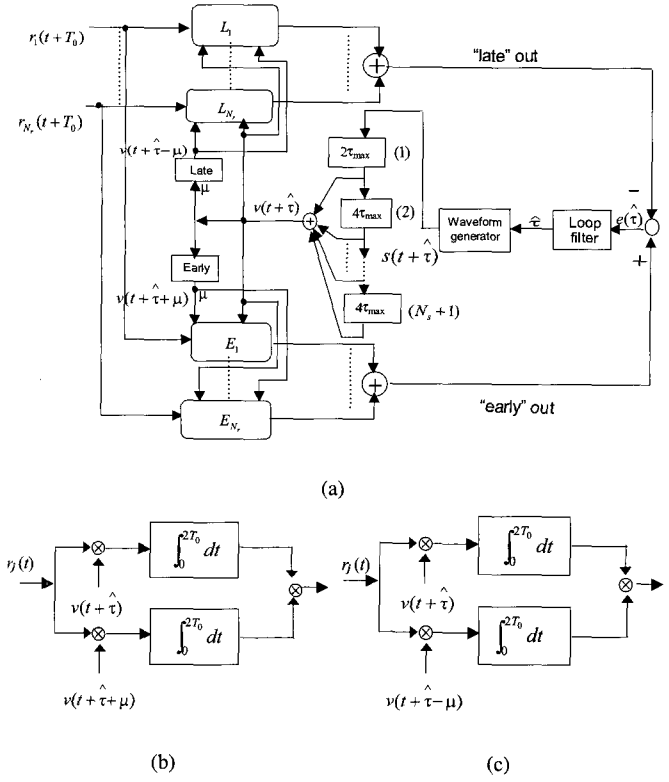

Fig. 1. (a) Block diagram of the overall noncoherent ML synchronizer, (b) block diagram of j-th correlator of the early-gate, (c) block diagram of j-th correlator of the late-gate.

being the reference signal and μ (sec) representing the early-late offset parameter. The first and second summations in (22) are the outputs of the "late" and "early" gates, respectively. A block diagram of the resulting synchronizer is reported in Fig. 1.

A. The Loop Filter

From an implementation point of view, the proposed early-late gate synchronizer is composed by a tapped-delay-line built up by $(1 + N_S)$ elements whose outputs are combined to feed two banks of N_r correlating blocks. In turn, each correlating block is composed by two analog correlators (see Figs.1(b) and 1(c)), so that $4N_r$ analog correlators are required to implement the synchronizer. Although analog or digital loop filters (LFs) could be employed for updating the reference signal $v(t + \hat{\tau})$ of Fig. 1(a), in the carried out numerical tests we have implemented 1st and 2nd order digital LFs to check the synchronizer performance.[7] Thus, after indicating as $e(m)$ and $\hat{\tau}(m)$ the input and output samples of the LF at the m-th iteration (e.g., at the instant $t = mD$), the input/output relationship for the 1st order LF is [28]

$$\hat{\tau}(m) = \hat{\tau}(m-1) + G_0 e(m)$$

while for the 2nd order LF we have [28] (see also Fig. 3(b))

$$\hat{\tau}(m) = 2\hat{\tau}(m-1) - \hat{\tau}(m-2) + (G_1 + G_2)e(m) - G_1 e(m-1).$$

[7]In order to update the $(1 + N_S)$ outputs of the tapped-delay-line present in Fig. 1(a), the delay D introduced by the LFs should be of the order of $2(1 + N_S)\bar{\tau}_{max}$.

Table 1. Optimized values for the coefficients of the 1st and 2nd order digital LFs. The signal acquisition operating scenario of Section IV-A has been considered.

$[\gamma(1+N_s)]$(dB)	G_0	G_1	G_2
5	8.012×10^{-2}	1.712×10^{-1}	1.712×10^{-1}
10	5.271×10^{-2}	1.235×10^{-1}	1.235×10^{-1}
15	8.012×10^{-3}	3.915×10^{-1}	3.915×10^{-1}
20	5.13×10^{-3}	8.151×10^{-3}	8.151×10^{-3}
25	2.01×10^{-3}	6.151×10^{-3}	6.151×10^{-3}
30	9.162×10^{-4}	1.141×10^{-3}	1.141×10^{-3}

About the optimized setting of the filter coefficients G_0, G_1, and G_2, we have tuned them according to the Jury's stability criterion [29], so as to give rise to LFs with stable close-loop transfer functions. In Table 1, we report the (numerically evaluated) optimized values of G_0, G_1, and G_2, for some $\gamma(1 + N_S)$ values of practical interest.

VI. SIMULATION SETUP AND NUMERICAL RESULTS

To test the performance of the proposed synchronizer, we have adopted the (unit-energy) monocycle in (20) as transmitted pulse $s(t)$ with a shaping factor T_s of 2.99 ns [2], [18], so that the resulting frequency spectrum of the pulse spans about 1.43 GHz around the 1.1 GHz center frequency. Values of $\bar{\tau}_{max}$ up to 50 ns have been considered and the early-late offset μ has been set to 0.15 ns. Without loss of generality, $N_S = 2$ has been considered in the simulations. Finally, the (numerically evaluated) performance plots we report in the next subsections have been averaged over 10^4 independent realizations of the fading coefficients $\{h_{j1},\ j = 1, \cdots, N_r\}$ of the SIMO channel. The performance of the proposed synchronizer has been checked under both signal acquisition and tracking operating conditions.

A. Signal Acquisition

In this operating condition, the actual value τ of the delay parameter has been randomly generated over the interval $[-\bar{\tau}_{max}, \bar{\tau}_{max}]$ and then held constant up to convergence of the synchronizer. The plots of Fig. 2 allow the comparison of the (numerically) evaluated mean squared error performance of the synchronizer of Fig. 1 against the corresponding CRB in (8) for increasing values of the number N_r of the receive antennas. These plots confirm that, even in the worst case of $N_r = 1$, SNRs γ of the order of 6.5 dB suffice to achieve the CRB. Furthermore, as predicted by (15), (19), for growing γ the convergence rate of the synchronizer performance toward the CRB increases by increasing the number N_r of the receive antennas, so that at $N_r = 6$ SNRs less than 5 dB suffice to achieve the CRB. Obviously, the steady-state performance reported in Fig. 2 does not depend on the order of the employed LF. However, we expect that the time (e.g., the number of iterations) required by the 2nd order LF for achieving the convergence is below that of the corresponding one demanded by the 1st order LF. In fact, the plots of Fig. 3 confirm this conclusion and show that, at SNRs γ around 10 dB, the convergence time of the 2nd order LF is about one-half that of the 1st order one.

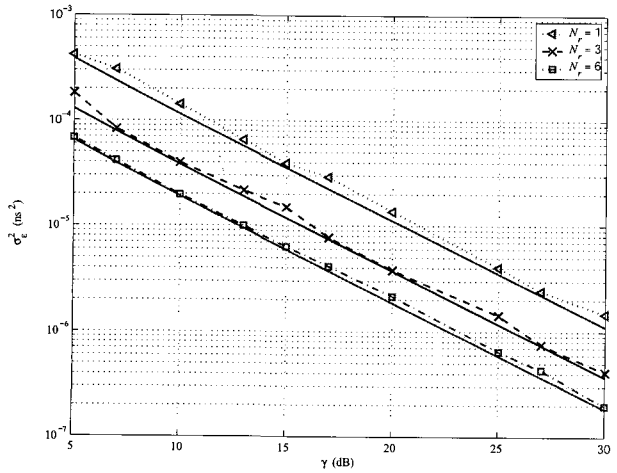

Fig. 2. Simulated mean squared errors of the synchronizer of Fig. 1 (dashed lines) versus the corresponding CRBs in (8) (continuous lines).

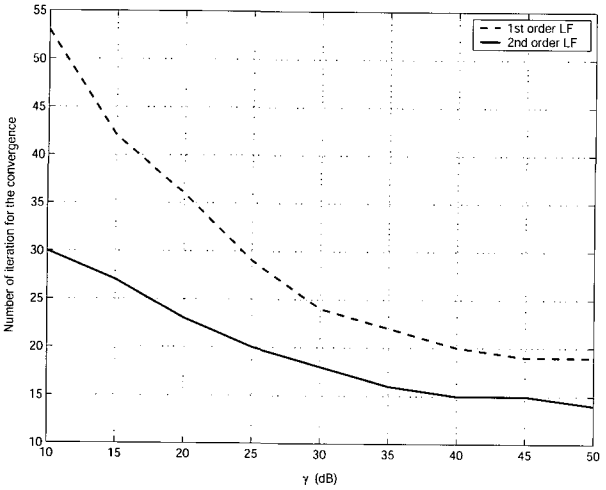

Fig. 3. Average number of iterations for the convergence of the 1st and 2nd order LFs systems with $N_r = 3$ receive antennas.

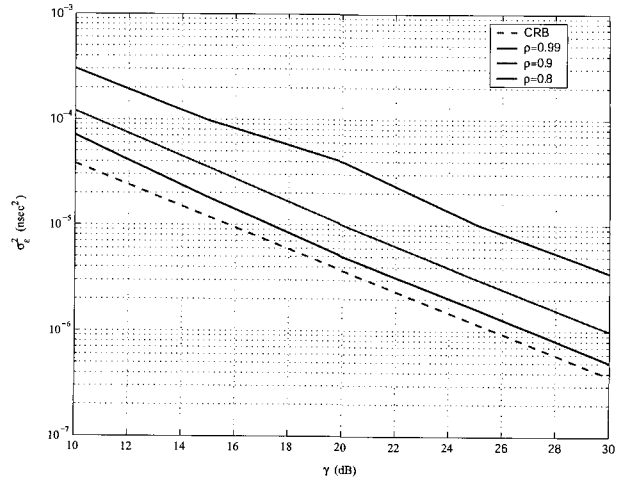

Fig. 4. Tracking performance of the proposed synchronizer equipped with the 1st order LF. $I_{\max} = 7$ and $N_r = 3$ have been considered .

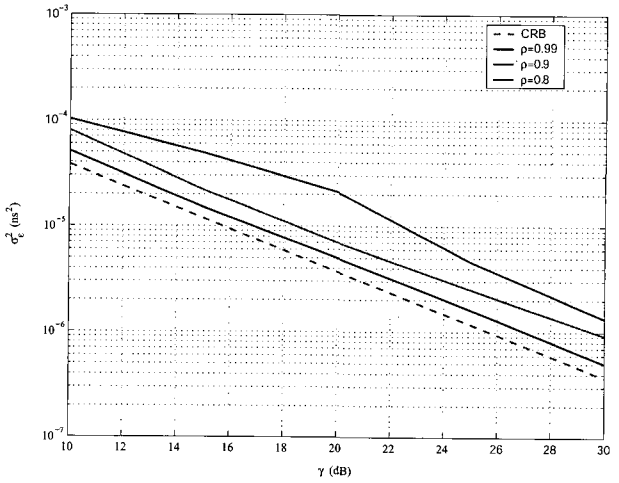

Fig. 5. Tracking performance of the proposed synchronizer equipped with the 2nd order LF. $I_{\max} = 7$ and $N_r = 3$ have been considered .

B. Tracking

The superiority of the 2nd order LF is also confirmed under tracking operating conditions. Specifically, to test the tracking performance of the proposed synchronizer, as in [18] we have modeled the jitter-affected delay parameter as a (stationary) zero-mean Gaussian random sequence $\{\tau(i)\}$, whose samples are generated at the (multiple of the) frame period T_0 in (3) according to the following relationship

$$\tau(i) = c\tau(i-1) + (1-c^2)w(i). \tag{23}$$

The sequence $\{w(i)\}$ in (24) is zero-mean, white, and Gaussian with standard deviation $\bar{\tau}_{\max}$, while the parameter $c \in [-1, +1]$ is the correlation coefficient $E\{\tau(i)\tau(i-1)\}/E\{\tau^2(i)\}$ of the Markovian series $\{\tau(i)\}$. Therefore, c may be set according to the fluctuation rate desired for the jitter.[8] To evaluate the performance of the 1st and 2nd order LFs on an equal footing, we have limited up to $I_{\max}$ the maximum number of iterations allowed to the LFs over each time interval T_0, and the performance plots achieved for $I_{\max} = 7$ have been drawn in Figs. 4 and 5 for c = 0.99, 0.9, and 0.8. As a benchmark, in these figures we have also plotted the corresponding CRB in (8). This CRB defines the (ultimate) performance achievable by the synchronizer under signal acquisition operating conditions, thus the gap between the simulated tracking performance and the CRB curves allows us to evaluate both the performance loss induced by the jitter and the tracking capability of the proposed synchronizer. A comparison of the performance plots of Figs. 4 and 5 confirms the enhanced tracking capability of the 2nd order LF, especially at low values of c (e.g., in the presence of fast jitter). In particular, at $c = 0.8$ the SNR gain of the 2nd order LF over the 1st order one is of about 3 dB for σ_ϵ^2 around 10^{-5} ns^2. Furthermore, the curve at $c = 0.8$ of Fig. 5 shows that at $\sigma_\epsilon^2 = 10^{-5}$ ns^2 the SNR penalty paid by the synchronizer performance equipped with 2nd order LF with respect to the CRB is just limited to 2.1 dB.

[8] Specifically, $c = 1$ gives arise to a maximally correlated time invariant (e.g., jitter free) sequence, while for $c = 0$ the sequence $\{\tau(i)\}$ reduces to the white series $\{w(i)\}$. So, the fluctuation rate of the generated jitter increases by passing from $c = 1$ to $c = 0$.

VII. CONCLUSIONS AND OPEN QUESTIONS

This contribution focused on the optimized design and performance evaluation of an ML synchronizer for multi-antenna fading-impaired UWB-IR transceivers with noncoherent reception. After deriving the CRB for the general case of MIMO UWB-IR systems, three transmit schemes of practical interest (namely, the SIMO, MIMO-ES, and MIMO-OS ones) have been compared in terms of the corresponding CRBs. Furthermore, the noncoherent ML synchronizer has been developed and analyzed for the SIMO transmit scheme which yields the lowest CRB. To this regard, since it is well known that orthogonal space-time MIMO signaling schemes achieve Shannon's capacity on MIMO faded channels, and (at medium/high SNR) minimize the bit error rate (BER) of the corresponding noncoherent ML detectors [3], [7], [20], [30], at a first glance it may be somewhat surprising that for timing recovery applications the MIMO-OS scheme of Section III-C fails to yield the lowest CRB. In fact, the ultimate BER performance of space-time noncoherent ML detectors is dictated by the corresponding Chernoff bound [30] and this last achieves its minimum when orthogonal signaling scheme (e.g., orthogonal space-time codes) are used. On the contrary, the analysis of the CRB of Section III seems to support the conjuncture that suitable correlation among the signals radiated by the transmit antennas may improve the ultimate synchronizer performance. However, the question about the *optimal design* of MIMO signaling schemes for timing recovery applications in faded environments is still open and this topic is currently investigated by the Authors.

APPENDIX I. DERIVATION OF THE CRB IN (5)

After introducing in Subsection A the vector representations of waveform MIMO channel in (1), we compute in Subsection B the likelihood function that will be employed in Subsection C to derive the CRB in (5).

A. The MIMO Vector Channel

By resorting to an L-dimensional orthonormal expansion complete for the N_t received signals in (1), the resulting L-dimensional (column) vector $\underline{\mathbf{r}}_j$ representing the received waveform $\{r_j(t),\ t \in [-T_0, T_0]\}$ is given by (see (1))

$$\underline{\mathbf{r}}_j = \sqrt{\frac{\gamma}{N_t}} \sum_{i=1}^{N_t} \sum_{m=-N_S/2}^{N_S/2} h_{ji}\, \underline{\mathbf{s}}_m^{(i)}(\tau) + \underline{\mathbf{n}}_j, \qquad j = 1, \cdots, N_r \quad \text{(A.1)}$$

where $\underline{\mathbf{s}}_m^{(i)}(\tau)$ is the L-dimensional vector representing the signal $s^{(i)}(t - 4m\bar{\tau}_{\max})$, while $\underline{\mathbf{n}}_j \sim \{\mathcal{N}(\underline{\mathbf{0}}_L, \underline{\mathbf{I}}_L)\}$ is the Gaussian vector corresponding to the noise waveform $\{n_j(t),\ t \in [-T_0, T_0]\}$ in (1). Therefore, after indicating as $\dot{\underline{\mathbf{s}}}_m^{(i)}(\bar{\tau})$ and $\ddot{\underline{\mathbf{s}}}_m^{(i)}(\bar{\tau})$ the L-dimensional vectors representing the first and second time derivatives of the signal $s^{(i)}(t - 4m\bar{\tau}_{\max})$, the following orthogonality relationships directly follow from (4)

$$\left(\underline{\mathbf{s}}_m^{(i)}(\tau)\right)^T \underline{\mathbf{s}}_l^{(j)}(\tau) = \delta(m,l)\varepsilon_{ss}(i,j), \quad \text{(A.2.1)}$$

$$\left(\dot{\underline{\mathbf{s}}}_m^{(i)}(\tau)\right)^T \dot{\underline{\mathbf{s}}}_l^{(j)}(\tau) = \delta(m,l)\varepsilon_{\dot{s}\dot{s}}(i,j), \quad \text{(A.2.2)}$$

$$\left(\underline{\mathbf{s}}_m^{(i)}(\tau)\right)^T \dot{\underline{\mathbf{s}}}_l^{(j)}(\tau) = \delta(m,l)\varepsilon_{s\dot{s}}(i,j), \quad \text{(A.2.3)}$$

$$\left(\underline{\mathbf{s}}_m^{(i)}(\tau)\right)^T \ddot{\underline{\mathbf{s}}}_l^{(j)}(\tau) = -\delta(m,l)\varepsilon_{s\dot{s}}(i,j) \quad \text{(A.2.4)}$$

where $\delta(m,l)$ is the Kronecker delta.

B. The Likelihood Function

Since the N_t vector observations $\underline{\mathbf{r}}_j$, $j = 1, \cdots, N_r$, in (A.1) are mutually independent conditional on τ, the resulting conditional joint pdf may be factorized as in

$$p(\underline{\mathbf{r}}_1, \cdots, \underline{\mathbf{r}}_{N_r} \mid \tau) = \prod_{j=1}^{N_r} p(\underline{\mathbf{r}}_j \mid \tau) = \prod_{j=1}^{N_r} \int p(\underline{\mathbf{r}}_j \mid \underline{\mathbf{h}}_j, \tau) p(\underline{\mathbf{h}}_j) d\underline{\mathbf{h}}_j \quad \text{(A.3)}$$

where $\underline{\mathbf{h}}_j \triangleq [h_{j1} \cdots h_{jN_t}]^T \sim \mathcal{N}(\underline{\mathbf{0}}_{N_t}; \underline{\mathbf{I}}_{N_t})$ is the N_t-dimensional (column) Gaussian vector gathering the MIMO channel coefficients from the N_t transmit antennas to the j-th receive one. Now, from (A.1) and the orthogonality property in (A.2.1) it follows that

$$p(\underline{\mathbf{r}}_j \mid \underline{\mathbf{h}}_j, \tau) = p(\underline{\mathbf{n}}_j = \underline{\mathbf{r}}_j - \sqrt{\frac{\gamma}{N_t}} \sum_{i=1}^{N_t} \sum_{m=-N_S/2}^{N_S/2} h_{ji}\, \underline{\mathbf{s}}_m^{(i)}(\tau)) = (2\pi)^{-L/2} \exp\left\{ -\frac{1}{2}\underline{\mathbf{r}}_j^T \underline{\mathbf{r}}_j + \sqrt{\frac{\gamma}{N_t}} \times \sum_{l=-N_S/2}^{N_S/2} \underline{\mathbf{h}}_j^T \underline{\mathbf{V}}_j^{(l)}(\tau) - \frac{1}{2}(1 + N_S)\frac{\gamma}{N_t} \underline{\mathbf{h}}_j^T \underline{\mathbf{Q}}_0 \underline{\mathbf{h}}_j \right\} \quad \text{(A.4)}$$

with the $(N_t \times 1)$ dummy vector $\underline{\mathbf{V}}_j^{(l)}(\tau)$ defined as

$$\underline{\mathbf{V}}_j^{(l)}(\tau) \triangleq [\underline{\mathbf{r}}_j^T \underline{\mathbf{s}}_l^{(1)}(\tau)) \cdots \underline{\mathbf{r}}_j^T \underline{\mathbf{s}}_l^{(N_t)}(\tau)]^T. \quad \text{(A.5)}$$

Therefore, by resorting to [25, (4.118)] for computing the N_t-variate Gaussian integrals present in the product (A.3), we arrive at the following final expression for the conditional joint pdf in (A.3)

$$p(\underline{\mathbf{r}}_1, \cdots, \underline{\mathbf{r}}_{N_r} \mid \tau) = \left(\sqrt{2\pi}\right)^{-(L+N_t)N_r} (\det[\mathbf{C}])^{-N_r/2} \times \exp\left\{ -\frac{1}{2} \sum_{j=1}^{N_r} \left[\underline{\mathbf{r}}_j^T \underline{\mathbf{r}}_j - \frac{\gamma}{N_t} \sum_{l=-N_S/2}^{N_S/2} \sum_{k=-N_S/2}^{N_S/2} \left(\underline{\mathbf{V}}_j^{(l)}(\tau)\right)^T \times \mathbf{C}^{-1} \underline{\mathbf{V}}_j^{(k)}(\tau) \right] \right\} \quad \text{(A.6)}$$

where the $(N_t \times N_t)$ matrix

$$\mathbf{C} \triangleq \mathbf{I}_{N_t} + \frac{\gamma}{N_t}(1 + N_S)\mathbb{Q}_0 \quad \text{(A.6.1)}$$

is symmetric and definite positive. So, after applying the lg (logarithmic) operator to the pdf in (A.6), the resulting first and second derivatives with respect to the delay parameter τ may be

expressed as in

$$\frac{\partial}{\partial\tau}\lg p(\underline{\mathbf{r}}_1,\cdots,\underline{\mathbf{r}}_{N_r}\mid\tau)=\frac{\gamma}{N_t}\sum_{j=1}^{N_r}\sum_{l=-N_S/2}^{N_S/2}\sum_{k=-N_S/2}^{N_S/2}\left(\underline{\mathbf{V}}_j^{(l)}(\tau)\right)^T \times\mathbf{C}^{-1}\dot{\underline{\mathbf{V}}}_j^{(k)}(\tau) \tag{A.7}$$

and

$$\frac{\partial^2}{\partial\tau^2}\lg p(\underline{\mathbf{r}}_1,\cdots,\underline{\mathbf{r}}_{N_r}\mid\tau)=\frac{\gamma}{N_t}\sum_{j=1}^{N_r}\sum_{l=-N_S/2}^{N_S/2}\sum_{k=-N_S/2}^{N_S/2} \times\left[\left(\dot{\underline{\mathbf{V}}}_j^{(l)}(\tau)\right)^T\times\mathbf{C}^{-1}\dot{\underline{\mathbf{V}}}_j^{(k)}(\tau)+\left(\underline{\mathbf{V}}_j^{(l)}(\tau)\right)^T\mathbf{C}^{-1}\ddot{\underline{\mathbf{V}}}_j^{(k)}(\tau)\right] \tag{A.8}$$

where the following auxiliary positions have been also introduced

$$\dot{\underline{\mathbf{V}}}_j^{(l)}(\tau)\triangleq\frac{\partial}{\partial\tau}\underline{\mathbf{V}}_j^{(l)}(\tau)=[\underline{\mathbf{r}}_j^T\dot{\underline{\mathbf{s}}}_l^{(1)}(\tau)\cdots\underline{\mathbf{r}}_j^T\dot{\underline{\mathbf{s}}}_l^{(N_t)}(\tau)]^T, \tag{A.9}$$

$$\ddot{\underline{\mathbf{V}}}_j^{(k)}(\tau)\triangleq\frac{\partial^2}{\partial\tau^2}\underline{\mathbf{V}}_j^{(k)}(\tau)=[\underline{\mathbf{r}}_j^T\ddot{\underline{\mathbf{s}}}_k^{(1)}(\tau)\cdots\underline{\mathbf{r}}_j^T\ddot{\underline{\mathbf{s}}}_k^{(N_t)}(\tau)]^T. \tag{A.10}$$

C. The CRB in (5)

Since the CRB for unbiased estimate of the delay parameter τ assumes the usual form

$$\sigma_\epsilon^2(\tau)\triangleq\mathrm{E}\left\{(\tau-\hat{\tau})^2\right\}\geq-\left[\mathrm{E}\left\{\frac{\partial^2}{\partial\tau^2}\lg p(\underline{\mathbf{r}}_1,\cdots,\underline{\mathbf{r}}_{N_r}\mid\tau)\right\}\right]^{-1} \tag{A.11}$$

we must carry out the expectation of (A.8) over the conditional joint pdf in (A.6). For this purpose, we apply the (general) property $\underline{\mathbf{a}}^T\underline{\mathbf{b}}=\mathrm{Tra}\{\underline{\mathbf{b}}\,\underline{\mathbf{a}}^T\}$ of the trace operator to the inner vector products in (A.8), so to rewrite them in the following equivalent forms

$$\left(\dot{\underline{\mathbf{V}}}_j^{(l)}(\tau)\right)^T\mathbf{C}^{-1}\underline{\mathbf{V}}_j^{(k)}(\tau)=\mathrm{Tra}\left\{\mathbf{C}^{-1/2}\mathbf{M}^{(j,\,k,\,l)}\mathbf{C}^{-1/2}\right\} \tag{A.12}$$

and

$$\left(\underline{\mathbf{V}}_j^{(l)}(\tau)\right)^T\mathbf{C}^{-1}\ddot{\underline{\mathbf{V}}}_j^{(k)}(\tau)=\mathrm{Tra}\left\{\mathbf{C}^{-1/2}\mathbf{F}^{(j,\,k,\,l)}\mathbf{C}^{-1/2}\right\} \tag{A.13}$$

where the following matrix positions have been also introduced

$$\mathbf{M}^{(j,\,k,\,l)}\triangleq\dot{\underline{\mathbf{V}}}_j^{(k)}(\tau)\left(\dot{\underline{\mathbf{V}}}_j^{(l)}(\tau)\right)^T, \tag{A.12.1}$$

$$\mathbf{F}^{(j,\,k,\,l)}\triangleq\ddot{\underline{\mathbf{V}}}_j^{(k)}(\tau)\left(\underline{\mathbf{V}}_j^{(l)}(\tau)\right)^T. \tag{A.13.1}$$

Now, by exploiting the orthogonality properties in (A.2.1)–(A.2.4), the expectations over the pdf in (A.6) of the above last matrices equate

$$E\left\{\mathbf{M}^{(j,\,k,\,l)}\right\}=(\gamma/N_t)\mathbf{Q}_1\mathbf{Q}_1^T+\delta(k,l)\mathbf{Q}_2, \tag{A.14}$$

$$E\left\{\mathbf{F}^{(j,\,k,\,l)}\right\}=-\left\{(\gamma/N_t)\mathbf{Q}_2\mathbf{Q}_0^T+\delta(k,l)\mathbf{Q}_2\right\} \tag{A.15}$$

for any combination of the $(j,\ k,\ l)$ indexes. Therefore, by exploiting the above expressions (A.14), (A.15) and resorting to the (general) property $\mathrm{Tra}\{\mathbf{AB}\}=\mathrm{Tra}\{\mathbf{BA}\}$ of the trace operator, the expectation of (A.8) can be computed as in

$$E\left\{\frac{\partial^2}{\partial\tau^2}\lg p(\underline{\mathbf{r}}_1,\cdots,\underline{\mathbf{r}}_{N_r}\mid\tau)\right\}=(\gamma(1+N_S)/N_t)^2N_r \times\mathrm{Tra}\left\{\left[\mathbf{Q}_2\mathbf{Q}_0^T-\mathbf{Q}_1\mathbf{Q}_1^T\right]\mathbf{C}^{-1}\right\}. \tag{A.16}$$

Finally, after inserting (A.6.1) in (A.16) and this last into (A.10), the CRB of (5) directly arises. □

APPENDIX II. DESCRIPTION OF THE EARLY-LATE GATE SYNCHRONIZER OF (21)

The early-late gate synchronizer constitutes an approximated implementation of the ML equation in (16) that, essentially, is based on the approximation of the time derivative $\dot{v}(t)$ of the signal (23) via the corresponding finite difference, i.e.,

$$\dot{v}(t)\triangleq\frac{dv(t)}{dt}\cong\frac{1}{2\mu}[v(t+\mu)-v(t-\mu)]. \tag{A.17}$$

Specifically, since cross-correlation functions are time shift invariant, we begin to rewrite (16) in the following equivalent form

$$\sum_{j=1}^{N_r}\left(\sum_{k=-N_S/2}^{N_S/2}\int_0^{2T_0}r_j(t+T_0)s(t+T_0+4k\bar{\tau}_{\max}+\hat{\tau}dt\right) \times\left(\sum_{l=-N_S/2}^{N_S/2}\int_0^{2T_0}r_j(t+T_0)\dot{s}(t+T_0+4l\bar{\tau}_{\max}+\hat{\tau}dt\right)\equiv 0. \tag{A.18}$$

Now, since $T_0-4k\bar{\tau}_{\max}=2(1+N_S-2k)\bar{\tau}_{\max}$, we may rewrite the summation over the k-index in (A.18) as in

$$\sum_{k=-N_S/2}^{N_S/2}\int_0^{2T_0}r_j(t+T_0)s(t+\hat{\tau}2\bar{\tau}_{\max}(2k-1))dt =\int_0^{2T_0}r_j(t+T_0)v(t+\hat{\tau})dt \tag{A.19}$$

with $v(t)$ being defined as in (23). By proceeding in an analogous way, the summation over the l-index in (A.18) may be expressed as in

$$\sum_{l=N_S/2}^{N_S/2}\int_0^{2T_0}r_j(t+T_0)\dot{s}(t+T_0-4l\bar{\tau}_{\max}+\hat{\tau})dt \equiv\int_0^{T_0}r_j(t+T_0)\dot{v}(t+\hat{\tau})dt. \tag{A.20}$$

Hence, after introducing (A.19) and (A.20) into (A.18), this

last assumes the following form

$$\sum_{j=1}^{N_r}\left(\int_0^{2T_0} r_j(t+T_0)v(t+\hat{\tau})dt\right) \times\left(\int_0^{2T_0} r_j(t+T_0)\dot{v}(t+\hat{\tau})dt\right)\equiv 0. \qquad \text{(A.21)}$$

Finally, after replacing the time derivative $\dot{v}(\cdot)$ in (A.21) by the corresponding finite difference (A.17), from (A.21) we directly arrive at (21).

□

REFERENCES

[1] M. Z. Win and R. A. Sholtz, "Impulse radio: How it works," *IEEE Commun. Lett.*, vol. 2, pp. 36–38, Feb. 1998.

[2] M. Win and R. A. Scholtz, "Ultra-wide bandwidth time hopping spread-spectrum impulse radio for wireless multiple access communications," *IEEE Trans. Commun.*, vol. 48, pp. 679–691, Apr. 2000.

[3] E. Baccarelli, M. Biagi, C. Pelizzoni, and P. F. Bellotti, "A novel multi-antenna impulse radio UWB transceiver for broadband high throughput 4G WLANs," *IEEE Commun. Lett.*, vol. 8, no. 7, pp. 419–421, July 2004.

[4] E. Baccarelli and M. Biagi, "An adptive codec for multiuser-interference mitigation for UWB-based WLANs," in *Proc. IEEE ICC 2003*, May 2003, pp. 2020–2024.

[5] Available at http://www.ieee802.org/15/pub/TG3a.html.

[6] R. A. Scholtz, "UWB radio deployment challenges," in *Proc. IEEE PIMRC 2000*, Sept. 2000, pp. 620–625.

[7] L. Yang and G. B. Giannakis, "Analog space-time coding for multiantenna ultra-wideband transmissions," *IEEE Trans. Commun.*, vol. 52, pp. 507–571, Mar. 2004.

[8] M. Pelissier, B. Denis, and D. Morche, "A methodology to investigate UWB digital receiver sensitivity to clock jitter," in *Proc. IEEE Conf. Ultra Wideband Syst. Technol.*, Nov. 2003, pp. 126–130.

[9] Z. Tian and G. B. Giannakis, "BER sensitivity to mis-timing in correlation based UWB receivers," in *Proc. IEEE GLOBECOM 2003*, Dec. 2003, pp. 441–445.

[10] I. Guvenc and H. Arslan, "Performance evaluation of UWB systems in the presence of timing jitter," in *Proc. IEEE Conf. Ultra Wideband Syst. Technol.*, Nov. 2003, pp. 136–141.

[11] L. Feng and W. Namgoong, "Joint estimation and detection of UWB signals with timing offset error and unknown channel," in *Proc. IEEE Conf. Ultra Wideband Syst. Technol.*, Nov. 2003, pp. 132–156.

[12] C. Carbonelli, U. Mengali, and U. Mitra, "Synchronization and channel estimation for UWB signals," in *Proc. IEEE GLOBECOM 2003*, Dec. 2003, pp. 764–768.

[13] G. M. Maggio and L. Reggianini, "A reduced-complexity acquisition algorithm for UWB impulse radio," in *Proc. IEEE Conf. Ultra Wideband Syst. Technol.*, Nov. 2003, pp. 131–135.

[14] Z. Tian and G. B. Giannakis, "Data-aided ML timing acquisition in ultra-wideband radios," in *Proc. IEEE Conf. Ultra Wideband Syst. Technol.*, Nov. 2003, pp. 142–146.

[15] L. Yang and G. B. Giannakis, "Low-complexity training for rapid timing acquisition in ultra-wideband communications," in *Proc. IEEE GLOBECOM 2003*, Dec. 2003, pp. 769–773.

[16] Y. Ma, F. Chin, B. Kannan, and S. Pasupthay, "Acquisition performance of an ultra-wideband fading channel," *IEEE Conf. Ultra Wideband Syst. Technol.*, May 2002, pp. 99–103.

[17] C. C. Chui and R. A. Scholtz, "Optimizing tracking loops for UWB monocycles," in *Proc. IEEE GLOBECOM 2000*, Dec. 2003, pp. 425–430.

[18] W. M. Lovelace and J. K. Townsend, "The effects of timing jitter and tracking on the performance of impulse radio," *IEEE JSAC 2002*, vol. 20, no. 9, pp. 1646–1651, Dec. 2002.

[19] M. Weisenhorn and W. Hirt, "Performance of binary antipodal signaling over indor UWB MIMO channel," in *Proc. IEEE ICC 2003*, vol. 4, May 2003, pp. 2872–2878.

[20] L. Yang and G. B. Giannakis, "Space-time coding for impulse radio," in *Proc. IEEE Conf. Ultra Wideband Syst. Technol.*, May 2002, pp. 235–239.

[21] P. Pajusco and P. Pagani, "Extension of SIMO wideband channel sounder for UWB propagation experiment," in *Proc. IEEE Conf. Ultra Wideband Syst. Technol.*, Nov. 2003, pp. 126–130.

[22] E. Baccarelli and M. Biagi, "A novel self-pilot based transmit-receiving architecture for multipath-impaired UWB systems," *IEEE Trans. Commun.*, vol. 52, no. 6, pp. 891–895, June 2004.

[23] J. Salz and J. H. Winters, "Effects of fading correlation on adaptive arrays in digital Mobile Radio," *IEEE Trans. Veh. Technol.*, pp. 1049–1057, Nov. 1994.

[24] S. Bregni, *Synchronization of Digital Telecommunications Networks*, Wiley, 2002.

[25] C. W. Helstrom, *Probability and Stochastic Processes for Engineers*, New York, USA, Prentice-Hall, 1998.

[26] H. V. Poor, *An Introduction to Signal Detection and Estimation*, 2nd ed., Springer-Verlag, 1994.

[27] U. Mengali and A. N. D'Andrea, *Synchronization Techniques for Digital Receivers*, New York, USA, Plenum, 1997.

[28] W. C. Lindsey, "A survey of digital phase-locked loops," *Proc. IEEE*, vol. 69, no. 4, pp. 410–431, Apr. 1981.

[29] E. I. Jury, *Theory and Application of the z-Transform Method*, New York, USA, Wiley, 1984.

[30] B. M. Hochwald and T. L. Mazzetta, "Unitary space-time modulation for multiple-antenna communication in Rayleigh flat fading," *IEEE Trans. Inform. Theory*, vol. 46, no. 2, pp. 543–564, Mar. 2000.

[31] S. S. Kolenchery, J. K. Townsend, J. A. Freebersyster, and G. Bilbro, "Performance of local power control in peer-to-peer impulse radio networks with bursty traffic," in *Proc. IEEE GLOBECOM'97*, Nov. 1997, pp. 910–916.

[32] E. Baccarelli, M. Biagi, and C. Pelizzoni, "A novel multi-antenna impulse radio UWB transceiver for broadband 4G WLANs," *Infocom Internal Tech. Report*, available at http://infocom.uniroma1.it/~biagi/mimouwbs.pdf.

Enzo Baccarelli received the Laurea degree (summa cum laude) in Electronic Engineering and Ph.D. degree in Communication Theory and Systems, both from the University La Sapienza, Rome, Italy, in 1989 and 1992, respectively. In 1995, he received the Post-Doctorate degree in Information Theory and Applications from INFOCOM Department, University La Sapienza, where he also served as Research Scientist from 1996 to 1998. Since 1998, he has been an associate professor in Signal Processing and Radio Communications at the University La Sapienza. From 1990 to 1995, he served as project manager at SELTI ELETTRONICA Corporation, Rome, where he worked on design of modems for high speed data transmissions. From 1996 to 1998, he attended the international project: AC-104: Mobile communication services for highspeed trainsMONSTRAIN, where he worked on equalization and coding for fast time varying radio-mobile links. Currently, he has been attending the international project SATURN, where he is involved in development of multiantenna-based high bit-rate HIPERLANtype wireless LANs. His research activities focus on the areas of systems design and coding, with specific interest in development and optimization of highperformance transmission/access systems for coded wireless/wired multimedia applications. He is the author of more than 60 international IEEE publications in these areas, and he currently serves as reviewer of several IEEE TRANSACTIONS, Journals, and Conferences. He is also co-author of two international patents on adaptive equalization and turbo-decoding for high speed wireless and wired data transmission systems licensed by international corporations.

Mauro Biagi was born in Rome in 1974. He received his "Laurea degree" in Telecommunication Engineering in 2001 from "La Sapienza" University of Rome. His research is focused on wireless communications (multiple antenna systems and ultrawide band transmission technology) mainly dealing with space-time coding techniques and power allocation/interference suppression in MIMO-ad-hoc networks with special attention to game theory applications. Concerning UWB his interests are focused on transceiver design and UWB-MIMO applications. His research is focused also on wireline communications and in particular bit loading algorithms and channel equalization for xDSL systems. He obtained the Ph.D. on Information and Communication Theory in January 2005, at INFOCOM Departmnt of the "La Sapienza" University of Rome. Actually, he is involved in the Italian National Project Wireless 802.16 Multi-antenna mEsh Networks (WOMEN) in project managing activities.

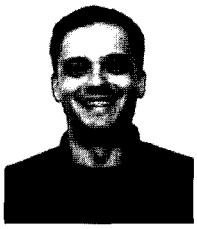

Cristian Pelizzoni was born in Rome, Italy, in 1977. He got the degree in 2003 in Telecommunication Engineering at University of Rome La Sapienza and he is currently a Ph.D student at the INFOCOM Department of the same university. He's involved in research activity about wireless communications, in particular, space time coding and game theory for ad-hoc networks and multi antenna ultra-wideband systems.

Nicola Cordeschi was born in Rome, Italy, in 1978. He received the Laurea degree(summa cum laude) in Telecommunication Engineering in 2004 from University of Rome "La Sapienza." He is pursuing the Ph.D. at the INFOCOM Department of the Engineering Faculty of "La Sapienza." His research activity focus on wireless communications, in particular dealing with the design and optimization of high performance transmission systems for wireless multimedia application, both in centralized and decentralized multiple antenna scenario.